IGTC2011-0194

Numerical Investigation of the Interaction between Probe, Flow and Blading in an Axial-Turbine

Florian Herbst[1], Sven Bluemel[1], Efstratios Fakiolas[2], and Joerg R. Seume[1]

[1] Institute of Turbomachinery and Fluid Dynamics
Leibniz University Hannover
Appelstrasse 9, 30167 Hannover, Germany

[2]Laboratory of Fluid Mechanics and Turbomachinery
Aristotle University of Thessaloniki
Thessaloniki, Greece

ABSTRACT

The measurement accuracy of pneumatic probes in turbomachinery is limited by their interaction with the flow and the blading especially in the small axial gaps between blades and vanes at high flow velocities. In the present paper, this issue is investigated by means of three-dimensional steady and unsteady RANS simulations of an axial turbine with a meshed pneumatic probe between stator 2 and rotor 2. The probe is "calibrated" numerically in a typical free-jet calibration duct. The numerical calibration data agrees very well with the experimental for moderate flow angles. By performing numerical "measurements" with the probe in the turbine rig and comparing the values with the flow field without probe, significant differences especially of the pitch angle values are shown. These can be traced back to displacement effects of the probe on the flow which are not compensated by the calibration procedure.

NOMENCLATURE

c	[m/s]	velocity	
d	[m]	diameter of the probe	
f	[Hz]	frequency	
k	[-]	reduced frequency	Eq. (1)
l	[m]	chord length	
Ma	[-]	Mach number	
Ma_{is}	[-]	isentropic Mach number	Eq. (9)
PAC	[-]	pitch angle coeffiecient	Eq. (4)
p	[Pa]	static pressure	
Re	[-]	Reynolds number	
S	[-]	Strouhal number	Eq. (2)
SPC	[-]	static pressure coefficient	Eq. (6)
T	[K]	static temperature	
TPC	[-]	total pressure coefficient	Eq. (5)
YAC	[-]	yaw angle coefficient	Eq. (3)
x, y, z	[m]	cartesian coordinates	
y^+	[-]	wall distance in wall coordinates	

Greek

α	[°]	yaw angle in probe coordinates
α_m	[°]	yaw angle in machine coordinates
γ	[°]	pitch angle in probe coordinates
γ_m	[°]	pitch angle in machine coordinates
Δ	[-]	difference
η_{is}	[-]	isentropic turbine efficiency
θ	[°]	circumferential angle
κ	[-]	heat capacity ratio
μ_t	[Pa s]	eddy viscosity
Π_t	[-]	total pressure ratio

Subscripts

ax	axial direction
MS	at mid-spand
Pr	value of Prandtl Pitot tube
t	total value
VS	vortex shedding
WoP	value of computation without probe
x	value at axial position x
$0.5lax$	at 50% axial chord length
1	value at blade inlet
$1/2/3/4$	value of pressure holes 1/2/3/4

Manuscript Received on 30 April, 2011

INTRODUCTION

The improvement of the overall performance of turbomachinery depends on reliable data describing the flow field inside the machine. In order to obtain these data experimentally pneumatic probes are widely used for measuring pressure, velocity, flow angle and, when supplied with a thermocouple, temperature. For this purpose, the probes are calibrated prior to the measurement campaign as a function of Mach number and flow angle in a steady and homogeneous flow of low turbulence [1-3]. Obviously, these conditions do not apply to the flow inside of turbomachinery: the flow is a priori unsteady and high velocity gradients in conjunction with an elevated turbulence level occur especially in the wake regions downstream of the blades. Furthermore, the implementation of the probe in the machine's duct causes a blockage effect which may lead to the measurement of distorted velocities and flow angles [1,4]. Additionally, Reynolds number effects are typically not covered by the probe's calibration procedure [1]. In sum all these characteristics may limit the valid range of application of pneumatic flow probes in turbomachinery for a given measurement accuracy.

Nevertheless, not all of these effects have the same significance. Whereas the turbulence level and Reynolds number have shown to have minor influence and may be corrected empirically [1], respectively, the gradient influence and the blockage effect as well as the steady and unsteady interaction between probe, flow and blading directly depend on the probe's and the measurement setup's design and have to be considered. Sitaram et al. [5] showed in order to limit the blading's wall influence on the probe a minimum dis-

tance of two probe-diameters has to be met. Furthermore, unsteady effects due to fluctuating velocities and flow angles like the dynamic circulation around the probe and the dynamic stall especially of wedge type probes depend on the reduced frequency

$$k = \frac{fd}{c}, \qquad (1)$$

and thus, on the probe's dimension. In this case f describes the frequency of a perturbation of the velocity field imposed on the probe, e.g. the blade passing frequency. The shedding frequencies of vortices at the probe's body - Kármán vortex street – for typical probe flows ($10^3 < \mathrm{Re} < 10^5$) is given with

$$S = \frac{f_{VS}d}{c} = 0.21 \qquad (2)$$

and hence, is also a function of the probe's diameter. Consequently, previous investigations (e.g. [4, 6]) have shown that a decrease of the probe's size is able to reduce systematic measurement errors (i.e. bias) of pneumatic probes caused by these numerous effects. However, to prevent intense reactions on the measurement accuracy, a synchronization of f and f_{VS} has to be avoided, when changing the probe's dimension [4]. It is therefore a second constraint for its miniaturization besides the obvious manufacturing limit.

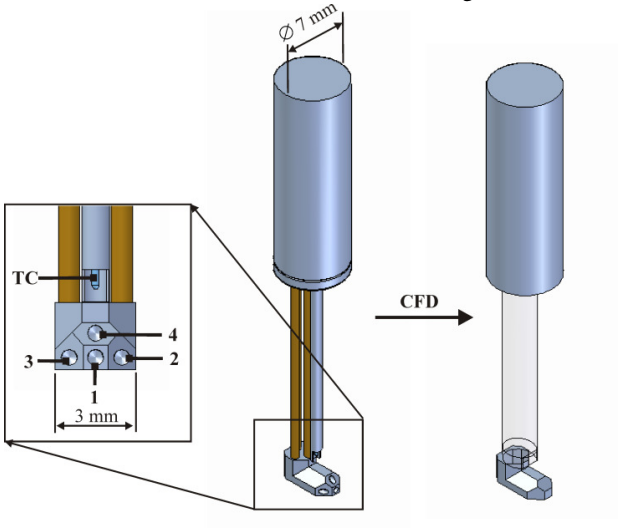

Fig. 1 Cobra-Probe hole numeration (left) and simplified CFD-geometry (right); TC: thermocouple; pressure hole diameter 0.6 mm

The current numerical study accompanies the preparations of a comprehensive measurement campaign at the institute's air-turbine test rig. Since the campaign's main subject is the investigation of the viscous and inviscid unsteady rotor-stator interaction as a function of a decreasing axial gap (of rotor and stator), the impact of a pneumatic probe on the flow should remain constantly small and the measurement accuracy high, respectively.

Previous investigations have shown that numerical simulations are a promising way to observe the interaction of probe, flow and blading in axial turbomachinery [7-9]. Malvija et al. [10] used comprehensive CFD simulations to deduce an optimal probe positioning in an automotive wheel arch with regard to increased measurement accuracy. Furthermore, De Guzmann et al. [11] extensively studied the flow around a four-hole cobra-probe numerically and validated the results successfully by comparing the probe's numerical and experimental calibration data. In order to proof the validity of the calibration procedure in the presence of the aerodynamic interactions in an axial-compressor, Coldrick et al. [9] conducted numerical probe measurements between the rotor and the stator and compared it to the flow values without probe. Seume et al. [7] showed in a similar setup that for this purpose experimental calibration data of the probe are insufficient – in fact a numerical calibration of the probe is obligatory. Various authors [12, 13] successfully used three-dimensional CFD methods for the design and calibration of pneumatic pressure probes. However, Restemeier et al. [14] showed by means of the design process of a miniaturized new five-hole probe that numerical simulations have to be applied with care. Due to a false prediction of separation zones their probe provided an unfavourable behaviour for small flow angles in the experimental validation.

In this baseline study, the validity of a free-jet calibration procedure is investigated by conducting numerical "measurements" by means of a typical steady pneumatic four-hole cobra-probe between stator 2 and rotor 2 in a two-stage axial turbine test rig. Since previous investigations have shown that different probe designs may lead to systematic deviations especially of the flow angles [15] the investigations will focus on the measurement bias of the current probe. Furthermore, the corresponding steady and unsteady, viscous and inviscid interactions between probe, flow and blading will be examined. Prior to these in-rig simulations the probe's aerodynamic behaviour is investigated using the numerical calibration setup of the probe.

FOUR-HOLE COBRA-PROBE

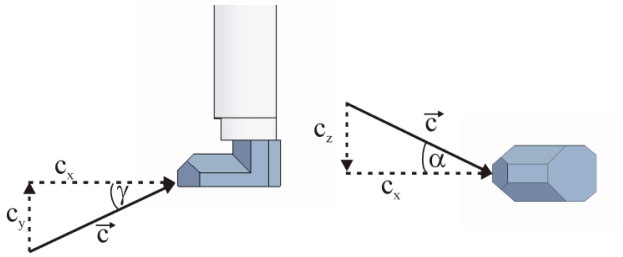

Fig. 2 Detail of simplified CFD-geometry and definition of the pitch angle γ (left) and the yaw angle α (right)

The steady measuring four-hole probe called "Probe E" is used for the current study. The cobra-type probe was developed for measurements in the near-hub region [2], which is indicated by the position of hole 4 above the total pressure hole 1 for measuring the pitch angle γ (Fig. 1 left). The probe consists of four small tubes, two central and two placed in a symmetrical arrangement. Each of these tubes is providing pressure values to a digital data logger. For measuring the flow's total temperature a thermocouple is placed above pressure hole 4.

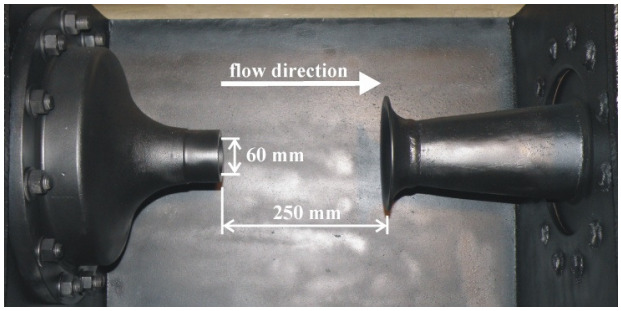

Fig. 3 Free jet region of the calibration duct

The head of the cobra probe, the flow angles, the velocity vector, and its three components are presented in Fig. 2. Since the flow around the probe depends on the conditions of the upstream flow and on the flow angles α and γ, the measured pressures in the pressure holes are not equal to the ones of the undisturbed flow field. Thus, proper calibration coefficients for the angles and the total and static pressure are defined and correlated to the values of an undisturbed, known flow field of a calibration duct. These coefficients are for α the yaw angle coefficient

$$YAC = \frac{p_2 - p_3}{p_1 - (p_2 + p_3)/2}, \qquad (3)$$

for γ the pitch angle coefficient

$$PAC = \frac{p_1 - p_4}{p_1 - (p_2 + p_3)/2}, \qquad (4)$$

for p_t the total pressure coefficient

$$TPC = \frac{p_{t,Pr} - p_1}{p_1 - (p_2 + p_3)/2}, \qquad (5)$$

and for p the static pressure coefficient

$$SPC = \frac{p_{Pr} - (p_2 + p_3)/2}{p_1 - (p_2 + p_3)/2}. \qquad (6)$$

The experimental calibration of the probe was conducted in the institute's high-speed calibration duct at an axial position of one nozzle diameter downstream of a convergent nozzle (Fig. 3) at the free jet's middle axis. For determining the calibration coefficients for a given *Ma*, α and γ are varied by rotating and tilting the probe around pressure hole 1. Reference values of the jet's total and static pressure are measured by a Prandtl Pitot tube parallel at the probe's axial position (see Eq. 5 and 6). The calibration duct allows a calibration for *Ma* up to 1.

PROBE CALIBRATION AND AERODYNAMICS

Numerical Model

For the CFD-simulations the geometry of the probe is simplified in accordance with Seume et al. [7], i.e.

- the four pressure holes are removed,
- the pressure tubes are replaced by a covering elliptic cylinder (Fig. 1 right), and
- the thermocouple is replaced by a step in this cylinder (Fig. 2 left).

With regard to the variation of the pitch and yaw angle these simplifications lead to a massive reduction of the effort for the mesh generation. The changes of the aerodynamic and measurement properties of the probe, in turn, are assumed to be negligible and acceptable, respectively, as the primary objective of the current work is not the direct comparison with experimental probe measurements.

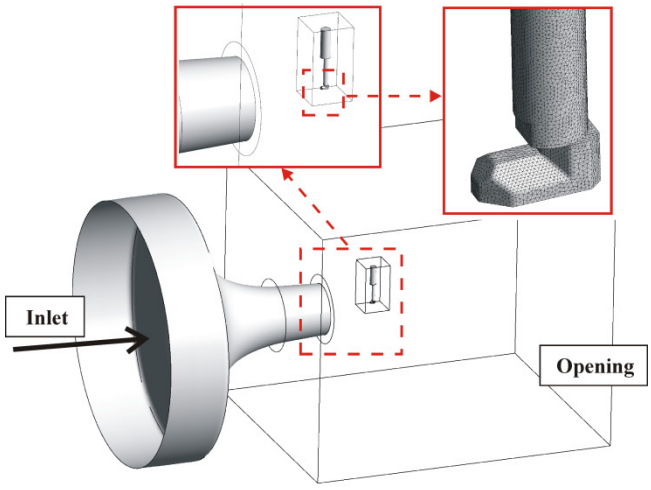

Fig. 4 Numerical model of the calibration duct and the probe

Furthermore, only the nozzle of the calibration duct is modelled, whereas the bellmouth (see Fig. 3 right) is replaced by a free volume of 50x40x40 probe shaft diameters size (Fig. 4) with opening boundary conditions (ambient static pressure). A comparison between the numerical and experimental radial total pressure profile of the free jet at the probe's calibration position confirms the validity of this assumption (not shown here).

In order to allow an easy variation of the probe's pitch and yaw angle the probe-near region (cubic region around probe in Fig. 4) is discretized using tetraeders and a prism-layer close to the wall. The nozzle as well as the free-jet region is discretized with a hexahedral mesh. The total number of grid points is about 2.5 million whereas all no-slip walls (nozzle and probe) are resolved with $y^+ < 2$.

The probe is experimentally calibrated in 2°-steps for -45° ≤ $\alpha, \gamma \leq$ 45°. For symmetrical reasons the numerical yaw angle calibration is only conducted for 0° ≤ $\alpha \leq$ 45°. The numerical pitch angle calibration is limited to the range -20° ≤ $\gamma \leq$ 45°. The numerical calibration is conducted in 5°-steps. Both calibrations are performed for *Ma* = 0.45 and *Ma* = 0.6, whereas only the first is shown here.

Only steady simulations of the calibration are performed with ANSYS CFX 12 using the SST turbulence model of Menter [16] and a 2nd order discretization scheme. All computations reached convergence with maximum residuals below 10^{-2}, RMS residuals below 10^{-4}, and a massflow imbalance below 0.001%.

Results

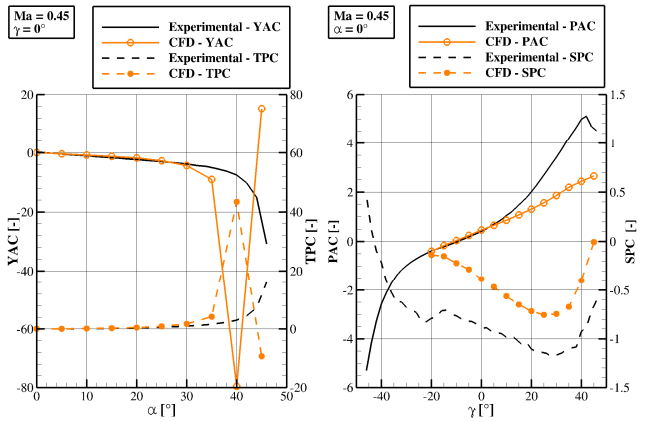

Fig. 5 Numerical and experimental calibration coefficients as a function of yaw (left) and pitch angle (right) for *Ma* = 0.45

In Fig. 5 a representative excerpt of the calibration data for *Ma* = 0.45 which is the relevant Mach number for measurements in the air-turbine is shown. At first, focussing on the yaw angle variation (Fig. 5 left) a very good agreement between the experimental and numerical calibration coefficients YAC and TPC can be observed for 0° ≤ $\alpha \leq$ 30°. For higher yaw angles the simulations are in no way able to reproduce the experimental results which can be traced back to the appearance of boundary layer separation at the probe's head near hole 2 (Fig. 6 lower right).

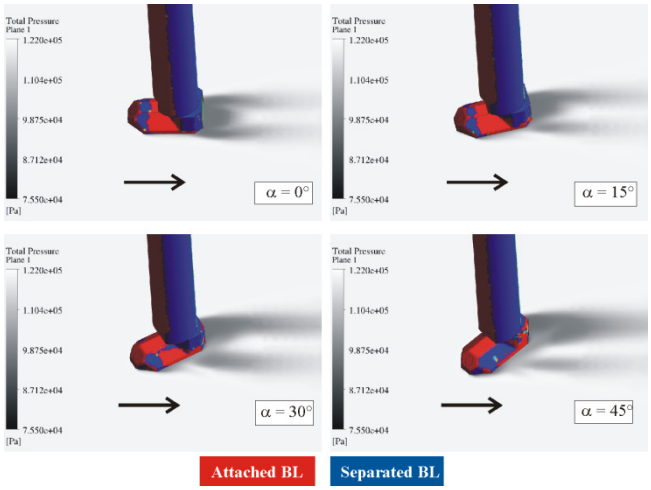

Fig. 6 Total pressure contour and status of probe boundary layer (derived from wall shear stress) as a function of yaw angle for *Ma* = 0.45 (main flow direction indicated)

With regard to the pitch angle variation (Fig. 5 right) a similar trend can be investigated. For PACs of -20°≤ γ≤ 15° experimental and numerical results match very well, for higher angles the numerical shows a linear, less steep behaviour than the experimental coefficient. Again a growing separation at the probe's head – this time near hole 4 – can be investigated (Fig. 7 lower left and right, recirculation zone in the total pressure contour).

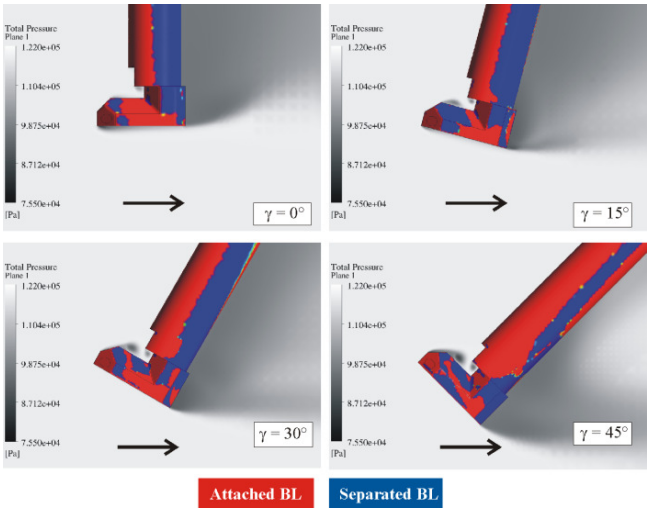

Fig. 7 Total pressure contour and status of probe boundary layer (derived from wall shear stress) as a function of pitch angle for Ma = 0.45 (main flow direction indicated)

Considering the well known shortcomings of RANS turbulence models (e.g. the SST model) in predicting open, non-reattaching separations the current results are not surprising. Hence, it has to be assumed, that for high incidences when separations occur at the pressure holes and numerical and experimental calibration coefficients differ significantly, the numerical results are not reliable. And, although not shown here in a detailed view, the good accordance of the PAC for $\gamma \leq -10°$ can also traced back to the occurrence and the non-occurrence, respectively, of separation at the pressure holes. In this case, the flow direction (from top left to lower right) leads to attaching boundary layers at the pressure holes despite of the high incidence.

Although at the time being no clear reason can be named, the nearly constant offset of the SPC values (Fig. 5 right) has to be mentioned. The deviation of this coefficient which is directly linked to static pressure gives rise to the assumption that there are probably deviations between the CAD/CFD and the real probe's geometry additionally to the simplifications of the CFD geometry. Nevertheless, the overall good accordance of the numerical and experimental calibration coefficients for the flow angles and the total pressure – besides the already mentioned differences for high incidences – emphasizes the reliability of the experimental and the numerical calibration. Furthermore, it shows in principal the validity of the simplification of the probe's geometry.

AIR-TURBINE TEST-RIG

For the investigation of the interaction of probe, flow and blading the two-stage air-turbine test rig of the Insitute of Turbomachinery and Fluid Dynamics is used. The two-stage configuration consists of the stages 3 and 4 of the four-stage test rig as described by Herzog et al. [17]. Fig. 8 shows the meridional sketch of the rig. The blading was designed in accordance with the free vortex law with a reaction ratio of 50% at mid-span. At the hub region of the rotor blades this results in a small reaction and high deflection whereas at the blade's tips a high reaction and a small deflection occur. The flow is subsonic over the full blade height. Further characteristics of the blading and the rig are given in Tab. 1.

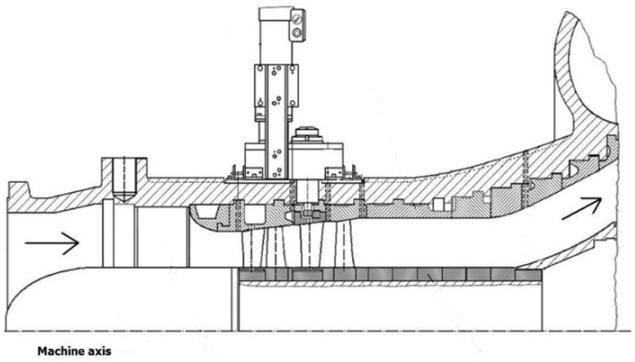

Fig. 8 Two-stage air-turbine test rig (flow direction indicated)

Tab. 1 Characteristics of the two-stage turbine at design point

Rotational speed n [min^{-1}]				7500
Net power P [kW]				300
Massflow $\dot{m}$ [kg/s]				7.8
Isentropic efficiency η_{is} [-]				0.913
Total temperature at inlet $T_{t,1}$ [K]				374
Total pressure at inlet $p_{t,1}$ [Pa]				167823
Total pressure ratio Π_t [-]				1.57
	stator 1	rotor 1	stator 2	rotor 2
Number of blades [-]	29	30	29	30
Reynolds number $Re \cdot 10^5$ [-]	6.1	5.1	5.1	4.7
Pitch $t_{MS,0.5cax}$ [mm]	67	66	69	67
Axial chord length $l_{ax,MS}$ [mm]	46	38	46	37
Axial gap (upstream) $b_{ax,MS}$ [mm]		9	23	25
Span $h_{0.5lax}$ [mm]	81	87	95	102
Reaction ratio r_{MS} [mm]	0.5		0.5	
Flow coefficient ϕ [-]	0.4		0.4	
Stage loading coefficient ψ [-]	1.0		0.9	

NUMERIAL PROBE MEASUREMENT

Numerical Model

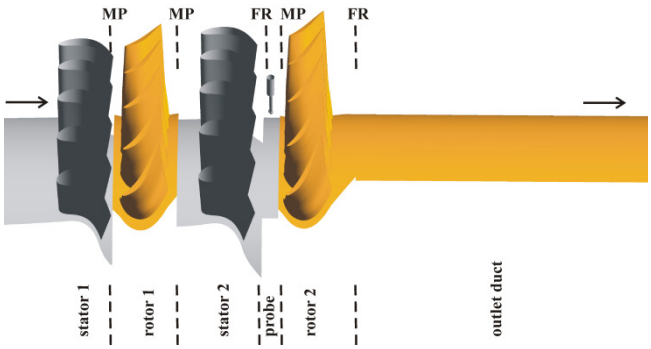

Fig. 9 Numerical setup of the steady simulations with probe, frame-change interfaces indicated (MP: mixing plane; FR: frozen rotor), and stationary (grey) and rotating walls (orange) marked (shroud not shown; main flow direction indicated)

The simulations of the probe-flow-blading interaction are conducted by means of a baseline mesh of the two-stage turbine without probe and of a modified mesh with probe. With regard to the unsteady computations, the number of stator blades is increased to 30 to ensure an equal pitch of rotating and stationary frames. Five pitches are simulated whereas at their circumferential boundaries rotational periodicity is applied (Fig. 9). The complete hexahedral mesh without probe consists of about 10 million grid points. All blade walls are resolved with $y^+ < 2$, hub and shroud walls with $2 < y^+ < 40$.

The interfaces between stator and rotor parts are modelled by mixing planes (MP) in the steady cases and with transient stage interfaces in the unsteady simulations. The probe block is linked upstream to stator 2 by a frozen rotor interface (FR) in both simulation types (Fig. 9). At the inlet constant massflow boundary condition and at the outlet an average static pressure is assumed. All computations are conducted at the design point of the turbine (see Tab. 1).

For the computations with probe the cubic mesh region around the probe (see Fig. 4) of the numerical calibration setup is implemented at 50% of the axial gap between stator and rotor 2 with hole 1 at 55% channel height. In order to avoid high yaw angle incidences the probe is rotated 55° counter-clockwise so that it is approximately aligned with the flow direction. At each circumferential direction a hexahedral block is added to the probe's block to fill up the five-pitch rotational periodic region. The total number of grid points of this setup increases to about 15 million – Fig. 10 gives an impression of the computational mesh with probe.

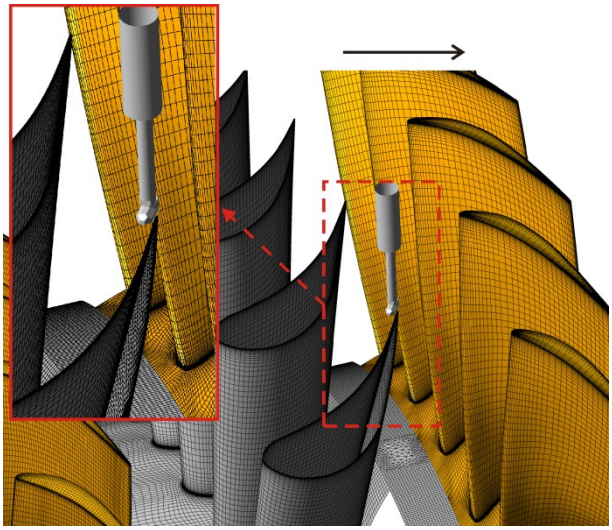

Fig. 10 Probe and surface mesh of stator 2 and rotor 2 including hub (mirror image shown for better visibility of probe; main flow direction indicated)

Note that the yaw and pitch angles shown in the following evaluation are in the coordinate system of the machine (turbine) whereas the probe measures in its previously defined relative coordinate system (see Fig. 2). Both coordinate systems are related by

$$\alpha_m = \alpha + 55° \qquad (7)$$

$$\gamma_m = \gamma. \qquad (8)$$

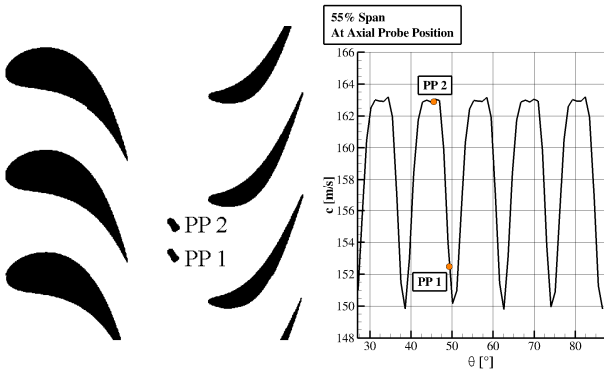

Fig. 11 Geometrical (left) and aerodynamic (right) probe positions (PP1: probe position 1; PP2: probe position 2)

Two circumferential positions of the probe are investigated in the steady simulations: position 1 (PP 1) at $\theta = 48.8°$ and position 2 (PP 2) at $\theta = 45.5°$ (Fig. 11 left). Whereas PP 1 lies directly in the wake of the upstream stator vane and thus, represents a region of high velocity gradients, PP 2 is placed in the more uniform main flow (Fig. 11 right). In order to quantify the unsteady interaction PP 1 and the setup without probe are also computed unsteadily.

For all simulations ANSYS CFX 13 with the SST turbulence model of Menter [16] and with a 2nd order discretization scheme is used. The steady and unsteady computations reached convergence with maximum residuals below 10^{-2}, RMS residuals below 10^{-4}, and a massflow imbalance below 0.001%. In the unsteady computations one full rotation of the rotor is simulated (simulation time: 0.008 s) resolving one pitch with 20 time steps (time step size: $1.33 \cdot 10^{-5}$ s).

Steady Results

By modelling five pitches and 60° of the turbine, respectively, and assuming rotational periodic boundary conditions the numerical setup is equal to a measurement with six probes equally distributed in circumferential direction. This modelling causes a blockage effect which is higher than in a typical experimental measurement setup where only one probe per axial position is used. Anyway, the influence of the six probes on the performance characteristic of the whole turbine is fairly low as Tab. 2 shows (constant massflow boundary condition applied). Thus, it can be assumed in the following that the numerical model with probe is a valid representation of the flow through the turbine rig for a typical measurement situation.

Tab. 2 Percentage change of turbine performance characteristics with probe referred to case without probe (steady computations)

	PP 1	PP 2
$\Delta\eta_{is,WoP}$ [%]	-0.239	-0.275
$\Delta\Pi_{t,WoP}$ [%]	0.264	0.003

In a first evaluation, the local flow values at the probe positions of the computation without probe are compared with the computations with probe. The probe values are obtained by using the previously presented numerical calibration data in an inverse procedure:

- At the positions of the pressure holes at the probe's head the four area averaged pressure values are determined.
- With these values local YAC and PAC values are calculated.
- The numerical calibration coefficients are approximated by polynomials of the 4th degree.
- The local α and γ are calculated with the local YAC and PAC as root of the polynomials.
- Finally p_t and p are calculated by TPC and SPC as a function of α and γ.
- The local density is calculated using the ideal gas law with the temperature determined at the position of the thermocouple.

Tab. 3 Local flow values at the probe positions 1 and 2 (steady computations)

	PP 1		PP 2	
	without probe	with probe	without probe	with probe
p_t [Pa]	137505	137510	139264	139300
p [Pa]	121874	122690	121205	123030
c [m/s]	152.48	153.86	163.37	161.01
α_m [°]	68.56	70.35	67.89	67.97
γ_m [°]	5.10	4.72	7.63	6.43

In Tab. 3 a comparison of the major local flow values with and

without probe at both probe positions is given. It has to be mentioned that in both positions both flow angles are within the reliable range for the RANS simulation, viz. no separations occur at the pressure holes. Only minor differences of the total pressure values can be observed, whereas the static pressures are measured 0.6% (PP 1) and 1.5% (PP 2) too high by the probe. Similar percentage deviations can be observed for the velocity. However, the absolute deviations of the yaw and the pitch angle are remarkably: the yaw angle is measured 1.79° (PP 1) and 0.08° (PP 2) too high, the pitch angle 0.38° (PP 1) and 1.2° (PP 2) too low. This level of deviation would be not tolerable for experimental measurements.

In order to verify the numerical measurement results, and especially in order to investigate the interactions of the probe with the flow the circumferential distributions of the local flow values 2 mm upstream the probe's head at 55% span are plotted. In Fig. 12 the distributions of the velocity magnitude for both probe positions are shown – positions are indicated – and in Fig. 13 additionally the pitch and yaw angle for position 1 are illustrated.

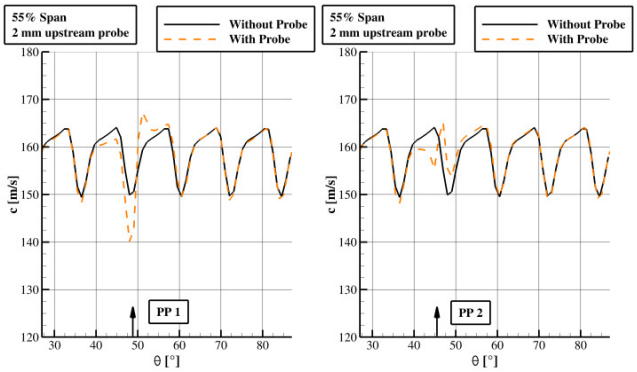

Fig. 12 Magnitude of velocity as a function of θ of probe position 1 (left) and 2 (right), 2 mm axial upstream of the probe at 55% span

Obviously, the displacement effect of the probe causes a local acceleration and deflection of the flow. This disturbance of the flow field is locally limited to three pitches, whereas the biggest impact can be identified in the pitch angle (Fig. 13 left). The latter can be mainly traced back to the blockage effect of the probe's shaft and the deflection of the flow below the probe. Anyway, the locally limited disturbances emphasize the assumption deduced from the turbine performance characteristics that modelling five pitches and six probes, respectively, is a valid representation of an experimental measurement situation.

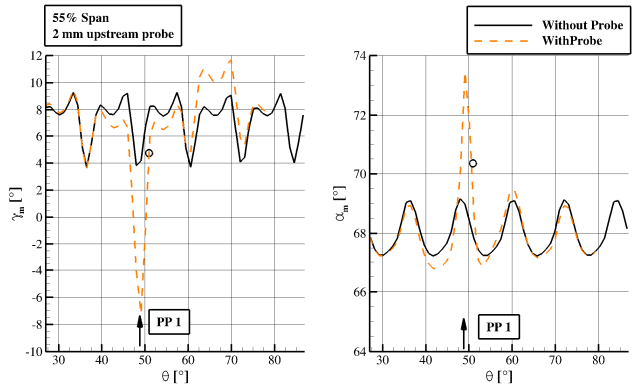

Fig. 13 Pitch angle (left) and yaw angle (right) as a function of θ at probe position 1, 2 mm axial upstream of the probe at 55% span; **o** indicates virtually shifted probe with measurement value of Tab. 3

For the purpose to correlate the probe measurement with the distributions taken 2 mm upstream of the probe the circumferential component of the velocity has to be considered, i.e. the probe position has to be shifted virtually in circumferential direction. By taking an approximate $\alpha_m = 68°$ (see Tab. 3) a virtual probe shift of $\Delta\theta = +2°$ can be estimated. In Fig. 13 this virtual shift together with probe measurement values of α_m and γ_m (Tab. 3) are indicated by a circle. Considering this shift the charts gives rise to the conclusion, that the values measured by the numerical probe (Tab. 3) are the flow values which are induced by the probe itself. Hence, the current calibration (data) seems not to be able to correct the influence of the probe on the flow. The measurement accuracy therefore depends on the probe's impact on the flow which is mainly a function of the probe's geometry and size, respectively. It is worth mentioning that the deviation of the measured yaw angles between a three- and a five-hole probe in an axial compressor as described by Janssen et al. [15] probably may be explained by these observations, too. Reasons for this behaviour might be the less dominating displacement effect of the probes in the free-jet calibration duct and the direct interaction with the blading in the turbomachine.

With regard to the latter the potential effect of the numerical probe on the blading is analyzed by means of the local isentropic surface Mach number

$$Ma_{is,x} = \sqrt{\frac{2}{\kappa-1}\left[\left(\frac{p_x}{p_{t,1}}\right)^{\frac{1-\kappa}{\kappa}} - 1\right]} \qquad (9)$$

on the closest stator vane upstream of probe position 1 (see Fig. 11 left). The distributions with probe are compared to the distributions without in Fig. 14. In order to quantify the effect of the probe's size two spanwise positions are investigated: at the probe's head at 55% span and at a height of the larger elliptic cylinder of the shaft (see Fig. 1 right) at 65% span. For both positions a minor but noticeable reduction of Ma_{is} on the profile's suction side can be observed between x_{ax}/l_{ax} = 0.4...1.0. The reduction is gradually increasing with decreasing distance to the probe and is generally higher for the larger spanwise position. Anyway, since the impact is rather small for this probe-blade distance of about 3...4 probe diameters the direct interaction with the stator blade plays a minor role for the measurement error of the numerical probe. When decreasing the axial gap between rotor and stator in future investigations this effect might increase and should be investigated again.

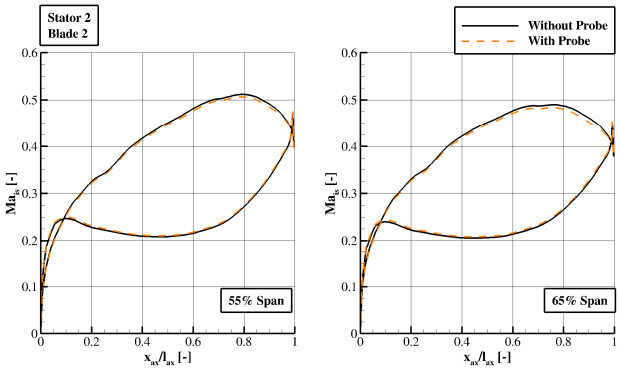

Fig. 14 Isentropic Mach number on stator blade 2 at two spanwise positions, PP 1

Unsteady Results

Tab. 4: Local flow values at the probe measurement position 1 (unsteady computations; values pitch-averaged)

	PP 1	
	without probe	with probe
p_t [Pa]	136780	136750
p [Pa]	121823	122360
c [m/s]	149.45	151.84
α_m [°]	67.92	70.41
γ_m [°]	5.72	4.65

Only steady computations have been performed so far which neglect the unsteady effects on the probe's measurement accuracy as described in the introduction. Since the probe at hand is a steadily measuring device the effects can be summarized in a

time-average of one pitch of the calibration coefficients. Tab. 4 shows the resulting main flow values of the simulations with and without the probe at position 1 (PP 1).

While total and static pressure as well as velocity magnitude deviate on a similar level like in the steady computations the deviations of the yaw angle (+2.49°) and of the pitch angle (-1.07°) further increase. Based on these results it can be concluded that downstream stator 2 in the current setup unsteady effects do not change the tendencies of the steady computations but further deteriorate the measurement accuracy of the flow angles.

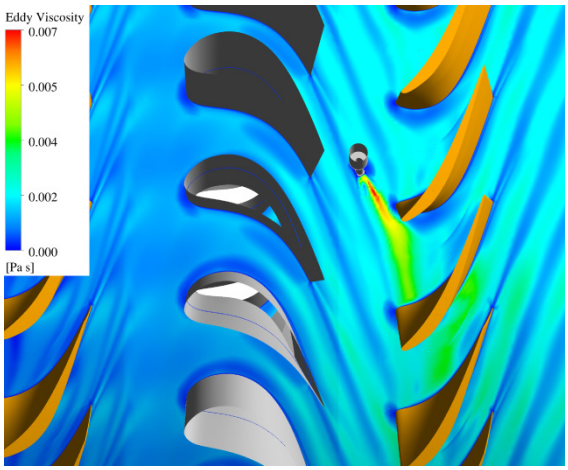

Fig. 15 Eddy viscosity contour plot at 55% span, snapshot of unsteady computation (PP 1)

However, a probe position downstream the rotor would probably face even more unsteady effects, at least due to the periodically impinging wakes. The wake influence of the probe on the rotor, in turn, is illustrated qualitatively in Fig. 15 by means of the eddy viscosity μ_t. Obviously, one rotor blade/passage faces a significant higher free-stream turbulence which is transported downstream. Anyway, as long as there are not a larger number of probes per axial position no noticeable effects (see Bohn et al. [1]) should occur.

CONCLUSIONS

The measurement accuracy of a pneumatic four-hole probe and its interaction with the blading and flow of an axial two-stage turbine was investigated by means of steady and unsteady RANS simulations with and without a meshed probe.

The probe was first calibrated experimentally and by steady simulations in a free-jet calibration duct. Both calibrations agree very well for moderate pitch and yaw angles which shows the validity of this typical pneumatic probe calibration facility. However, for higher incidences, the RANS simulations are not able to reproduce the experimental values due to the wrong prediction of separations close to the probe's pressure holes. An offset of the static pressure calibration coefficient seems to be due to deviations between the CFD and the experimental probe geometries.

By using the numerical calibration data, probe measurements at two distinct circumferential positions between stator 2 and rotor 2 of the two-stage turbine were conducted in the steady simulations with probe. The comparison with the flow field of the simulation without probe shows deviations depending on the probe's position of about maximum 1.5% for all flow values besides the flow angles. The yaw angle as well as the pitch angle deviates up to 1.8° which would not be tolerable for experimental measurements.

It could be shown that the deviations are caused by the displacement effect of the probe on the flow. Hence, the calibration procedure in the free-jet duct is not able to capture these effects.

In an unsteady computation with probe the tendencies of the steady results were confirmed although the deviations of the flow angles are even higher.

In order to improve measurement accuracy, future investigations should put effort into the development of calibration procedures which are able to compensate the probe's effects on the flow in turbomachinery flow passages. The current numerical setup and simulations offer a starting point for these improvements. For example, further circumferential and radial probe positions might be computed in order to find correlations between the relative probe position and the measurement uncertainty. Furthermore, the further deterioration of the measurement accuracy by unsteady effects as well as the characteristics of different probe designs (e.g. cylindrical probes), sizes, and shaft shapes should be analyzed.

ACKNOWLEDGMENTS

The author's gratefully acknowledge the valuable contributions of their colleagues Arne Vorreiter concerning the calibration duct as well as Marc Biester and Michael Henke concerning the turbine test-rig. Furthermore, we thank Lasse Müller for creating the baseline mesh of the two-stage turbine and ANSYS for providing CFX, Turbogrid and ICEM CFD in an academic license. Finally, we acknowledge the valuable suggestions of the anonymous reviewers.

REFERENCES

[1] Bohn, D., Funke, H., Heuer, T., 2000, "Sonden-Schaufel-Interaktion bei stationären Messungen mit pneumatischen Strömungssonden in engen Axialspalten," *FVV Final Report,* Vol. 688-2.

[2] Rieß, W., Braun, M., 2003,"Stationäres und instationäres Verhalten verschiedener Typen von Strömungs-Messsonden in instationärer Strömung," *DFG Final Report*, Ri 375/13-1, Institute of Turbomachinery and Fluid Dynamics, Leibniz Universität Hannover, Germany.

[3] Saravanamuttoo, H. I. H. (ed.), 1990, "Recommended practices for measurement of gas path pressures and temperatures for performance assessment of aircraft turbine engines and components," *AGARD Advisory Report,* No. 245.

[4] Humm, H. J., 1996, "Optimierung der Sondengestalt für aerodynamische Messungen in hochgradig fluktuierenden Strömungen," *Ph.D Thesis*, Eidgenösische Technische Hochschule Zürich, Switzerland.

[5] Sitaram, N., Lakshminarayana, B., Ravindranath, A., 1981," Conventional Probes for the Relative Flow Measurement in a Turbomachinery Rotor Blade Passage," *Journal of Engineering for Power*, Vol. 103, No. 2, pp. 406-414.

[6] Humm, H. J., Gossweiler, C. R., Gyarmathy, G., 1995, "On Fast-Response Probes: Part 2—Aerodynamic Probe Design Studies," *Journal of Turbomachinery*, Vol. 117, No. 4, 618-624.

[7] Seume, J.R., Herbst, F., Missirlis, D., Yakinthos, K., Goulas, A., 2006, "Numerical model of the unsteady interaction between probe and flow in axial turbomachinery", *Proceedings XVIII Symposium on Measuring Techniques in Turbomachinery Transonic and Supersonic Flow in Cascades and Turbomachines*, Thessaloniki, Greece.

[8] Coldrick, S., Ivey, P. C., Wells, R.G., 2004, "The Influence of Compressor Aerodynamics on Pressure Probes – Part 1: In Rig Calibrations," *Proceedings of ASME Turbo Expo 2004*, no. GT2004-53240.

[9] Coldrick, S., Ivey, P. C., Wells, R.G., 2004, "The Influence of Compressor Aerodynamics on Pressure Probes – Part 2: Numerical Models," *Proceedings of ASME Turbo Expo 2004*, No. GT2004-53241.

[10] Malviya, V., Mishra, R., Palmer, E., 2010, "CFD Investigation on 3-Dimensional Interference of a Five-Hole Probe in an Automotive Wheel Arch", *Advances in Mechanical Engineering*, Vol. 2010, No. 763718.

[11] De Guzmann, M. M., Fletcher, C. A. J., Hooper, J. D., 1994, "Computational Investigation of Cobra Probe Operation," *International Journal of Numerical Methods for Heat and Fluid Flow*, Vol. 4, pp. 425-445.

[12] Milanovic, I. M., Kalkhoran, I. M., 2000, "Numerical Calibration of a conical five-hole probe for supersonic measure-

ments", *Measurement Science Technology*, Vol. 11, pp. 1812-1818.

[13] Kim, S.-H., Kang, Y.-J., Myong, R.-S., Cho, T.-H., Park, Y.-M., Choi, I.H., 2009, "Calibration of a Five-Hole Multi-Function Probe for Helicopter Air Data Sensors", *International Journal of Aeronautical & Space Sciences*, Vol. 10, No. 2, pp. 43-51.

[14] Restemeier, M., Niewöhner, T., Pöhler, T., Jeschke, P., 2010, "Grenzen der numerischen Auslegung von minitaurisierten pneumatischen Sonden zur Strömungsfeldmessung", German *Aerospace Congress 2010*, No. 161328.

[15] Janssen, M., Seume J., Hönen, H., Lösch-Schloms, R., Gallus, H.E., 1993, „Flow Field Analysis of the Axial Compressor of the Siemens V84.3", *20th International Congress on Combustion Engines*, London, UK.

[16] Menter, F. R., 1994, "Two-Equation Eddy-Viscosity Turbulence Models for Engineering Applications," *AIAA Journal*, Vol. 32, No. 8, pp. 1598 – 1605.

[17] Herzog, N., Gündogdu, Y., Kang, G., Seume, J., Rothe, K., 2005, "Part-Load Operation of a Four-Stage Turbine," *Proceedings of ASME Turbo Expo 2005*, no. GT2005-68700